PERIODICO di MINERALOGIA
established in 1930

DIPARTIMENTO DI SCIENZE DELLA TERRA
SAPIENZA UNIVERSITÀ DI ROMA

An International Journal of
Mineralogy, Crystallography, Geochemistry,
Ore Deposits, Petrology, Volcanology
and applied topics on Environment, Archaeometry and Cultural Heritage

Petrogenesis of gabbroic rocks from the Malayer plutonic complex (Sanandaj-Sirjan zone, west Iran)

Amir Esna-Ashari [1,*] and Massimo Tiepolo [2]

[1] Department of Geology, Payame Noor University (PNU), PO Box 19395-3697, Tehran, Iran
[2] Department of Earth Sciences "A. Desio", University of Milano, Via Botticelli 23, Milano 20133, Italy

ARTICLE INFO

Submitted: January 2019
Accepted: October 2019
Available on line: November 2019

* Corresponding author:
amires@pnu.ac.ir

DOI: 10.2451/2020PM843

How to cite this article:
Esna-Ashari A. and Tiepolo M. (2020)
Period. Mineral. 89, 91-104

ABSTRACT

The Sanandaj-Sirjan zone (SSZ), extending from northwest to southeast of Iran, is a continental arc developed during subduction of the Neotethyan oceanic crust below the Central Iran microcontinent. The Malayer plutonic complex (MPC) is located in northern half of the SSZ and is characterized by the occurrence of subduction-related ultramafic to felsic rocks. Calculated composition of the melts in equilibrium with minerals from the gabbroic rocks were compared with the literature whole rock data from the MPC and from other neighboring complexes in the SSZ. The results showed that the parental melts at the origin of the gabbroic rocks is a high-Mg andesite (HMA) with a sanukitoid geochemical affinity originated by a melt-rock reaction process between a felsic melt and ultramafic rocks. This study further confirms that although ultramafic rocks are not commonly found associated with subduction-related rocks, their petrogenetic role cannot be underestimated.

Keywords: boninite; sanukitoid; gabbro genesis; melt-rock interaction; Sanandaj-Sirjan zone.

INTRODUCTION

Subduction of the oceanic crust below the continental crust is associated with voluminous intrusions in the forearc side of the continental arcs (e.g. Stern, 2002). Here, the felsic rocks are the most common and mafic rocks are generally subordinated. The latter are however of particular importance because the most informative on the nature of the sub-arc mantle and the processes responsible for magma genesis.

The composition of the primary arc magma mostly depends on the chemistry of the source components including the nature of the mantle wedge and of the subducted crust. A minor magma type in arcs is high-Mg andesites (HMAs). Despite the rare occurrence, HMAs are of great importance because their composition is very similar to the average composition of the continental crust and they may had contributed in some way to the formation of crust during the Archean (e.g. Kelemen, 1995).

HMAs are characterized by silica content comparable with that of andesites but with Mg# (Mg/Mg+Fe)>0.6 and high Ni and Cr contents. Boninite, adakite and sanukitoid are subgroups of HMAs with distinctive geochemical features. Boninite is the product of hydrous partial melting of a highly depleted mantle wedge during the onset of subduction (Crawford et al., 1989; Falloon and Danyushevsky, 2000). Sanukitoid generates through equilibrium reaction of mantle peridotite with silicic melts (Yogodzinski et al., 1994; Shimoda et al., 1998; Tiepolo and Tribuzio, 2008). Adakite is the product of partial melting of the subducted basaltic oceanic crust in eclogite facies with minor interaction with mantle peridotite (e.g. Kay, 1978; Defant and Drummond, 1990; Yogodzinski et al., 1995; Stern and Kilian, 1996).

The presence of HMAs was recently proposed in the Aligoodarz plutonic complex (APC) in the northern sector of the Sanandaj-Sirjan zone (SSZ) of Iran (Figure 1; Esna-Ashari et al., 2016). The APC together with Boroujerd plutonic complex (BPC) is mostly granitoid (granite to granodiorite) in composition with subordinate quartz-diorite and formed in the Middle Jurassic (Ahmadi-Khalaji, 2006; Esna-Ashari et al., 2012). The APC is characterized by the occurrence of ultramafic rocks (hornblendite and pyroxenite) that were proposed to be derived from a boninitic magma formed during the onset of subduction in Late Triassic-Early Jurassic. During Middle Jurassic, in a more mature setting, the newly formed acidic magma interacted with the ultramafic boninitic rock and produced a new intermediate quartz-dioritic magma comparable with the HMAs (Esna-Ashari et al., 2016).

In this study, we present new mineral chemistry data from gabbroic rocks of the Malayer plutonic complex (MPC) which is an intrusive complex close to the APC. The compositions of the melts in equilibrium with minerals were calculated and compared with the literature whole rock chemical data from the MPC gabbroic rocks. In addition, the MPC data are compared with those from other intrusive rocks in the northern half of the SSZ in order to shed more light on the genesis of the gabbro. This investigation reports for the first time the occurrence of ultramafic rock with boninitic affinity in the MPC. The genetic link between the ultramafic rock and a more evolved intermediate magma comparable in composition with the sanukitoid is discussed. In addition, it is shown that the parental liquid at the origin of gabbros is the result of interaction between ultramafic rock and an intermediate melt.

GEOLOGICAL SETTING

SSZ with the length of about 1500 km and a width that reaches up to 200 km is extended from northwest to southeast of Iran. It is a continental arc that resulted from subduction of Neotethys oceanic crust below the Central Iran microcontinent (e.g. Berberian and King, 1981; Agard et al., 2011; Hassanzadeh and Wernicke, 2016). The subduction was associated with the generation of widespread subduction-related magma and occurrence of regional and contact metamorphic rocks. The onset of subduction proposed to be Late Triassic-Early Jurassic (Arvin et al., 2007) and the continental collision occurred in Oligocene (Agard et al., 2011). The onset of subduction is characterized by sporadic occurrence of magmatic rocks in different parts of the SSZ (Arvin et al., 2007; Esna-Ashari et al., 2016) but the main phase of magmatism was related to Middle Jurassic (Ahmadi-Khalaji, 2006; Shahbazi et al., 2010; Ahadnejad et al., 2011; Esna-Ashari et al., 2011, 2012).

The MPC is located in the northern half of the SSZ western Iran (Figure 1) and is characterized by the widespread occurrence of felsic rocks. Mafic rocks are subordinated and the ultramafic rocks are rare. Mafic rocks occur either as gabbroic dikes or more voluminous gabbroic intrusions. Deevsalar et al. (2014, 2017, 2018a) proposed that the MPC intruded the continental crust in response to the subduction of the Neotethyan oceanic lithosphere below the Central Iran microcontinent in Middle Jurassic time. In particular, mafic melts originated as a consequence of the partial melting of a mantle wedge consisting of a metasomatized amphibole-bearing garnet-spinel lherzolite. Granitoid rocks were the results of partial melting of the continental crust in response to the heating provided by the intrusion of the mafic magma (Deevsaral et al., 2014, 2017, 2018a). Age determination of felsic to mafic rocks revealed intrusion of magma at three different times. One is coeval with the onset of subduction (~187 Ma; Ahadnejad et al., 2011) and the other is coeval with a more mature stage of the subduction in Middle Jurassic (169-173 Ma; Ahadnejad et al., 2011; Deevsalar et al., 2017). The youngest rocks (38 to 40 Ma) formed after subduction of the Neo-Tethyan ridge and subsequent magmatism following the slab break-off (Deevsalar et al., 2017, 2018b).

The largest mafic body of the MPC is the Tangsaran intrusion covering an area of about 1.6 km^2 (Figure 1c). Whole rock and major element mineral composition from the Tangsaran gabbro are reported in Deevsalar et al., (2014, 2017). We carried out sampling in different parts of the intrusion and most of the collected samples are amphibole-rich. Locally mafic rocks darker in color, showing extensive alteration and characterized by the occurrence of olivine and clinopyroxene were found (Figure 2).

EXPERIMENTAL

Major and trace element abundances were measured in olivine, pyroxene, amphibole, and plagioclase (Tables 1 and 2). Major element mineral chemistry was determined at the Department of Earth Sciences "A. Desio" of the University of Milano with a Jeol 8200 Superprobe. Accelerating voltage and beam current were set at 15 kV and 15 nA, respectively. Natural minerals were used as standards.

Trace element composition of the plagioclase, pyroxene and amphibole were determined by laser ablation inductively coupled plasma mass spectrometry (LA-ICP-MS) at the C.N.R. - Istituto di Geoscienze e Georisorse (IGG)-UOS of Pavia. The instrument couples a 266 nm Nd:YAG laser microprobe (Brilliant, Quantel) to a quadrupole ICP-MS system (DRCe from PerkinElmer). NIST-SRM612 was used as an external standard, whereas

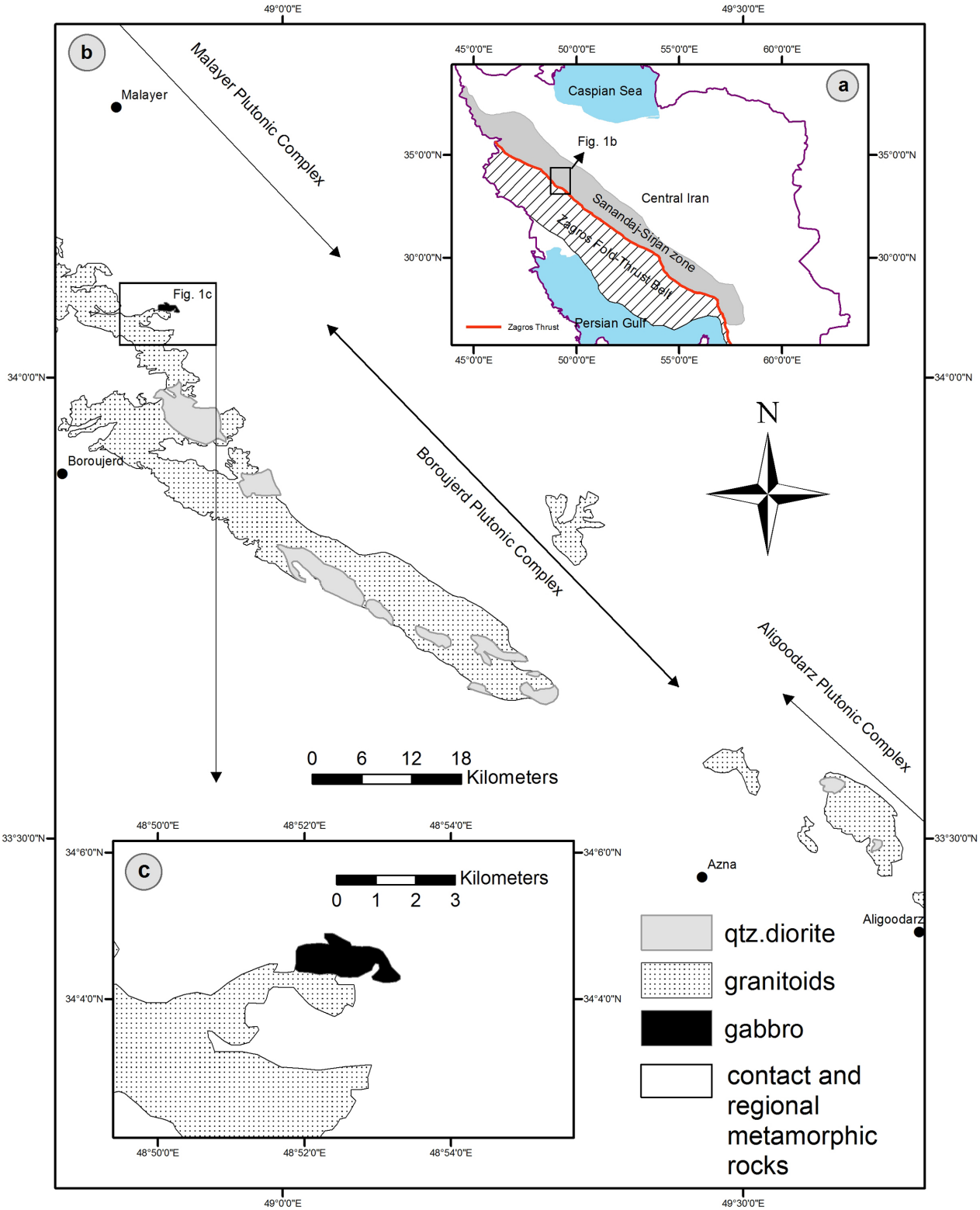

Figure 1. a) map of Iran showing the location of Sanandaj-Sirjan zone; b) part of the Sanandaj-Sirjan zone that is characterized by the occurrence of widespread plutonic complexes including Malayer, Boroujerd and Aligoodarz plutonic complexes (MPC, BPC, and APC respectively). c) a simple map showing part of the MPC and location of the Tangsaran gabbro intrusion.

Figure 2. Typical outcrops of the MPC gabbroic rocks.

^{43}Ca or ^{29}Si were adopted as internal standards, depending on the analyzed mineral. In each analytical run, the USGS reference sample BCR2 was analyzed together with the unknowns for quality control. Precision and accuracy are better than 5% and 10%, respectively. Major and trace element mineral compositions are presented in Tables 1 and 2.

PETROGRAPHY

Mafic rocks show granular texture and are medium to coarse-grained (grain size up to 2 mm). They are gabbroid in composition consisting of olivine, clinopyroxene, amphibole and plagioclase. Biotite is subordinate (Figure 3) and apatite and opaques are minor phases normally enclosed in other minerals.

Olivine occurs only in few samples generally highly fractured and altered to serpentine. It has coarser grain size relative to the other minerals and is characterized by lobate shape and rounded boundaries. Reaction corona around the olivine is a common feature. Major element measurement of the reaction corona revealed that it is composed of pyroxene and chlorite (Deevsalar et al., 2014). This suggests that the olivine is not in equilibrium with the surrounding minerals.

Clinopyroxene is present in few samples and mostly associated with olivine. It has euhedral to anhedral shapes and is partly replaced by amphibole. It occurs either as separate minerals or as small inclusions in amphibole oikocryst.

Amphibole is the most abundant mafic mineral. It occurs mostly as single grain but sometimes poikilitically enclose or partly rim the small grains of plagioclase and pyroxene. Occasionally amphibole fills the interstitial space of olivine grains. Amphibole is occasionally altered to biotite and chlorite.

Plagioclase is anhedral to euhedral and occurs either as separate minerals or as inclusion in amphibole. It also occurs as an anhedral interstitial mineral. Sericitization of plagioclase is relatively common.

Rarely aggregates of cumulus olivine, amphibole and pyroxene can be seen in the gabbro. The aggregates show textural features different from other parts of the rock. Minerals in the aggregates are coarser-grained and they are devoid of plagioclase that is common in the gabbro. The aggregates seem to be fragments of an ultramafic rock enclosed into the gabbro. The boundary of these fragments are resorbed and surrounded by reaction corona (Figure 3d) suggesting disequilibrium with the surrounding gabbroic mineral assemblage.

MINERAL CHEMISTRY

Olivine shows Fo contents ranging from 0.75 to 0.79 mol. Variation of MnO is from 0.321 to 0.384 wt% and NiO from 0.003 to 0.021wt%.

Clinopyroxene is diopside in composition (Figure 4). It shows Mg# (Molar Mg/[Mg+Fe]) values in the range 0.85-0.86. TiO_2 is lower than 0.26 wt% and Al_2O_3 varies from 1.24 to 2.06 wt%. NiO is lower than 0.07 wt% whereas Cr_2O_3 content ranges from 0.272 to 0.400 wt%.

The chondrite-normalized REE patterns of the clinopyroxenes are almost flat (average Ce_N/Yb_N=1.31; Figure 5) with HREE at about 9 times CI chondrite. The chondrite-normalized incompatible trace element patterns of the clinopyroxene is characterized by negative Nb and Pb anomalies relative to the neighboring elements.

Amphiboles are pargasitic to edenitic hornblende (Figure 4). They are characterized by no significant Mg# variation (0.79 to 0.84). Al_2O_3 is in the range 10.7-13.1 wt% and TiO_2 is up to 2.86 wt%. NiO is less than 0.057 wt%.

The chondrite-normalized REE pattern of amphibole is characterized by slight LREE enrichment over HREE (Ce_N/Yb_N=2.5) which are almost flat (Dy_N/Yb_N=1.4) at about 20 times CI chondrite. The chondrite-normalized

Table 1. Major elements composition (wt%) of olivine, clinopyroxene, amphibole, and plagioclase.

	olivine						clinopyroxene					amphibole					plagioclase		
	1	2	3	4	5		1	2	3	4		1	2	3	4		1	2	3
SiO_2	38.740	39.070	40.420	38.620	38.760	SiO_2	53.250	53.860	53.460	53.150	SiO_2	48.490	47.270	46.460	44.070	SiO_2	45.310	45.760	45.530
TiO_2	0.033	0.037	bdl	bdl	0.042	TiO_2	0.214	0.116	0.156	0.258	TiO_2	0.046	bdl	bdl	2.860	TiO_2	0.032	bdl	0.038
Al_2O_3	bdl	bdl	bdl	bdl	bdl	Al_2O_3	2.060	1.319	1.245	1.325	Al_2O_3	10.670	12.910	12.890	13.130	Al_2O_3	36.190	35.930	36.050
Cr_2O_3	bdl	bdl	0.014	0.020	0.031	Cr_2O_3	0.400	0.323	0.398	0.272	Cr_2O_3	0.101	bdl	bdl	0.947	Cr_2O_3	bdl	bdl	bdl
FeOT	23.420	23.660	18.630	23.050	23.060	FeOT	5.020	4.730	4.760	4.720	FeOT	6.300	6.010	6.030	7.280	FeOT	0.076	0.217	0.059
MnO	0.325	0.384	0.321	0.378	0.367	MnO	0.136	0.183	0.207	0.241	MnO	0.070	0.100	0.098	0.120	MnO	0.050	0.002	0.018
NiO	0.014	0.017	0.010	0.021	0.003	NiO	0.070	bdl	bdl	bdl	NiO	bdl	bdl	0.048	0.057	NiO	bdl	0.065	0.049
MgO	39.080	39.170	38.290	39.230	39.220	MgO	15.990	15.920	15.820	15.980	MgO	17.700	17.090	17.310	14.940	MgO	bdl	0.011	bdl
CaO	bdl	bdl	0.051	0.023	0.016	CaO	22.790	22.860	23.150	23.610	CaO	12.020	12.260	12.300	12.100	CaO	18.290	18.060	18.120
Na_2O	bdl	bdl	0.014	0.009	0.003	Na_2O	0.143	0.090	0.100	0.108	Na_2O	1.580	1.880	2.000	1.590	Na_2O	1.031	1.133	1.119
K_2O	0.010	0.000	0.010	bdl	0.008	K_2O	0.002	bdl	0.011	bdl5	K_2O	0.285	0.023	0.010	0.868	K_2O	0.010	0.008	0.010
Total	101.622	102.337	97.760	101.351	101.509	Total	100.076	99.401	99.306	99.663	Total	97.261	97.543	97.146	97.962	Total	100.989	101.186	100.993
(apfu)						(apfu)					(apfu)					(apfu)			
Si	2.579	2.601	2.691	2.571	2.580	Si	1.952	1.982	1.974	1.960	Si	7.169	6.964	6.892	6.597	Si	1.034	1.042	1.038
Ti	0.002	0.002	----	----	0.002	Ti	0.006	0.003	0.004	0.007	Ti	0.005	----	----	0.322	Ti	0.001	----	0.001
Al	----	----	----	----	----	Al	0.089	0.057	0.054	0.058	Al	1.860	2.242	2.254	2.317	Al	0.973	0.964	0.969
Cr	----	----	0.001	0.001	0.001	Cr	0.012	0.009	0.012	0.008	Cr	0.012	----	----	0.112	Cr	----	----	----
FeT	0.652	0.659	0.519	0.642	0.642	FeT	0.154	0.146	0.147	0.146	FeT	0.779	0.741	0.748	0.911	FeT	0.001	0.004	0.001
Mn	0.009	0.011	0.009	0.011	0.010	Mn	0.004	0.006	0.006	0.008	Mn^{2+}	0.009	0.013	0.012	0.015	Mn	0.001	----	----
Ni	----	----	----	0.001	----	Ni	0.002	----	----	----	Ni	----	----	0.006	0.007	Ni	----	0.001	0.001
Mg	1.939	1.944	1.900	1.947	1.946	Mg	0.874	0.873	0.871	0.878	Mg	3.898	3.750	3.825	3.331	Mg	----	----	----
Ca	----	----	0.002	0.001	0.001	Ca	0.895	0.901	0.916	0.933	Ca	1.904	1.935	1.955	1.941	Ca	0.447	0.440	0.443
Na	----	----	----	----	----	Na	0.010	0.006	0.007	0.008	Na	0.453	0.537	0.575	0.461	Na	0.046	0.050	0.049
K	----	----	----	----	----	K	----	----	0.001	----	K	0.054	0.004	0.002	0.166	K	----	----	----
Fo	0.75	0.75	0.79	0.75	0.75	Mg#	0.850	0.857	0.856	0.858	Mg#	0.83	0.84	0.84	0.79	An	90.7	89.8	89.9
																Ab	9.25	10.19	10.05

bdl= below detection limit.

Table 2. Trace elements composition (ppm) of clinopyroxene, amphibole and plagioclase.

	clinopyroxene					amphibole		plagioclase				
	1	2	3	4	5	1	2	1	2	3	4	5
Li	2.83	11.6	8.65	9.17	10.2	2.30	3.39	1.21	3.97	8.01	21.7	12.8
Sc	85.7	112	219	99.6	108	147	146	1.57	2.41	2.34	6.15	bdl
V	383	612	1314	424	453	1225	1248	5.33	1.96	2.68	18.9	4.63
Cr	1687	3521	11377	1719	1960	4721	5149	bdl	3.42	bdl	75.7	15.4
Co	69.8	25.6	49.6	21.8	22.8	35.7	31.1	0.990	0.156	0.770	5.900	0.290
Ni	45.6	16.4	30.7	12.9	16.7	27.3	18.2	2.46	0.770	1.38	8.10	4.46
Zn	77.4	23.7	40.0	49.6	18.0	49.3	43.3	6.33	5.56	7.72	35.4	3.11
Rb	9.34	1.56	4.36	0.160	0.620	3.90	3.45	0.521	1.39	bdl	1.06	5.51
Sr	115	32.3	80.9	23.3	22.1	147	152	447	692	684	592	744
Y	6.29	8.46	24.5	7.17	8.11	19.3	17.5	0.265	0.040	bdl	0.370	bdl
Zr	6.45	8.58	37.6	10.5	11.6	33.8	30.4	1.58	0.620	0.450	bdl	2.07
Nb	0.249	0.107	0.317	bdl	bdl	10.3	8.39	0.244	bdl	0.072	bdl	0.330
Cs	0.061	0.413	0.127	bdl	0.336	bdl	bdl	0.045	0.257	0.952	2.28	6.14
Ba	77.0	5.99	35.8	bdl	2.91	105	102	35.9	52.8	52.9	32.9	95.2
La	6.30	1.60	5.18	1.39	1.20	4.76	5.10	1.52	1.50	1.39	1.56	1.73
Ce	15.5	5.91	18.2	3.60	4.58	17.3	17.7	3.19	2.04	2.69	3.35	3.36
Pr	1.94	1.10	2.90	0.650	0.940	2.97	2.53	0.270	0.189	0.146	0.237	0.244
Nd	7.65	5.16	15.0	3.69	5.92	14.0	13.4	0.450	0.410	0.830	1.010	bdl
Sm	1.86	1.46	4.07	1.24	0.580	4.90	4.88	0.097	bdl	bdl	bdl	bdl
Eu	1.22	0.459	0.895	bdl	0.450	0.760	1.37	0.521	0.615	0.754	bdl	0.520
Gd	1.07	1.18	4.74	0.370	1.64	5.11	3.56	0.123	0.112	bdl	bdl	bdl
Tb	0.192	0.270	0.631	0.230	0.327	0.461	0.441	bdl	bdl	bdl	bdl	bdl
Dy	1.27	1.64	4.68	0.750	2.79	4.46	3.26	0.073	bdl	bdl	bdl	bdl
Ho	0.249	0.332	1.15	0.184	0.332	0.780	0.630	0.015	bdl	bdl	bdl	bdl
Er	0.530	0.910	2.84	1.33	1.04	1.60	2.35	bdl	bdl	bdl	bdl	bdl
Tm	0.055	0.107	0.311	0.179	0.137	0.260	0.280	0.017	bdl	bdl	bdl	bdl
Yb	1.05	0.469	2.35	1.08	1.21	1.97	1.54	0.217	bdl	0.108	bdl	bdl
Lu	0.179	0.063	0.412	0.054	0.092	0.240	0.258	bdl	bdl	bdl	bdl	bdl
Hf	0.147	0.524	1.82	0.260	0.670	1.52	1.62	bdl	bdl	0.084	bdl	bdl
Ta	bdl	0.046	0.110	0.133	bdl	0.651	0.534	0.018	0.019	bdl	bdl	0.091
Pb	0.687	0.195	0.941	bdl	0.610	0.630	0.760	1.40	1.99	1.36	2.04	3.07
Th	1.30	0.228	0.505	0.278	0.089	0.215	0.105	0.942	0.126	0.332	0.090	bdl
U	0.601	0.082	0.258	0.050	0.040	bdl	0.117	0.243	0.043	0.119	bdl	0.052

bdl=below detection limit.

incompatible trace element pattern is characterized by Nb, Ta and Ti enrichment and Th, La, Pb and Zr depletion relative to the neighboring elements (Figure 5).

Plagioclase is anorthite 0.9 and has very low concentrations of trace elements with the exceptions of Sr and Ba which are up to 744 ppm and 95 ppm, respectively.

DISCUSSION

Equilibrium melt calculation

Occurrence of cumulus or xenocrystic minerals in the rocks cause the bulk rock chemistry to be not fully informative on the chemistry of the parental liquid composition. Nonetheless, by using trace element composition of the minerals and applying a consistent

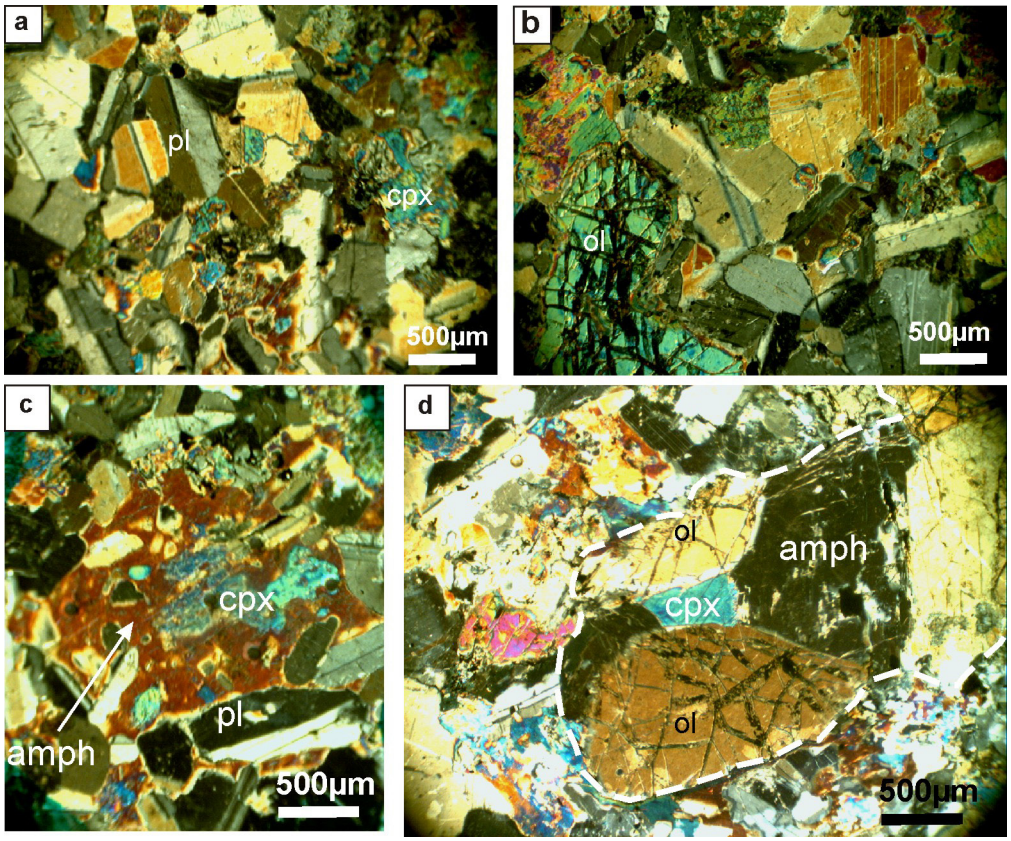

Figure 3. Microphotographs showing the textural features in the MPC gabbro. (a) variation of shape and size of plagioclase grains; (b) an olivine grain with a rounded shape and lobate boundary; (c) large grain of amphibole enclosing inclusions of clinopyroxene and plagioclase; d) fragment of cumulus minerals surrounded by a white dashed line in a fine-grained matrix. All pictures are taken in cross-polarized light.

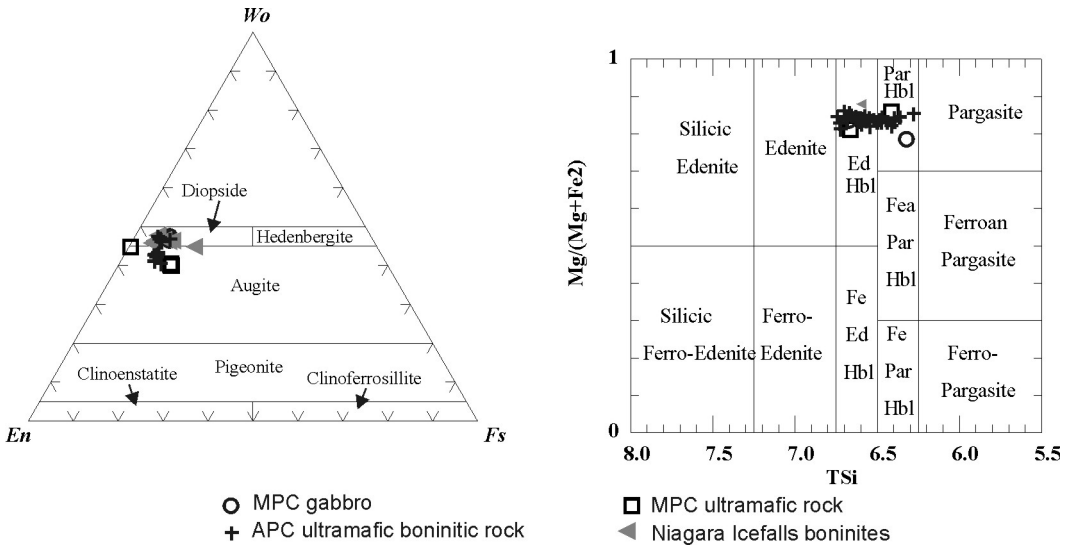

Figure 4. Diagrams showing the classification of clinopyroxene and amphibole from the MPC gabbroic and ultramafic rocks. Boninitic rocks from the APC (Esna-Ashari et al., 2016) and Niagara Icefalls (Tribuzio et al., 2008) are reported for comparison. Data for the MPC ultramafic rock is from Deevsalar et al. (2014).

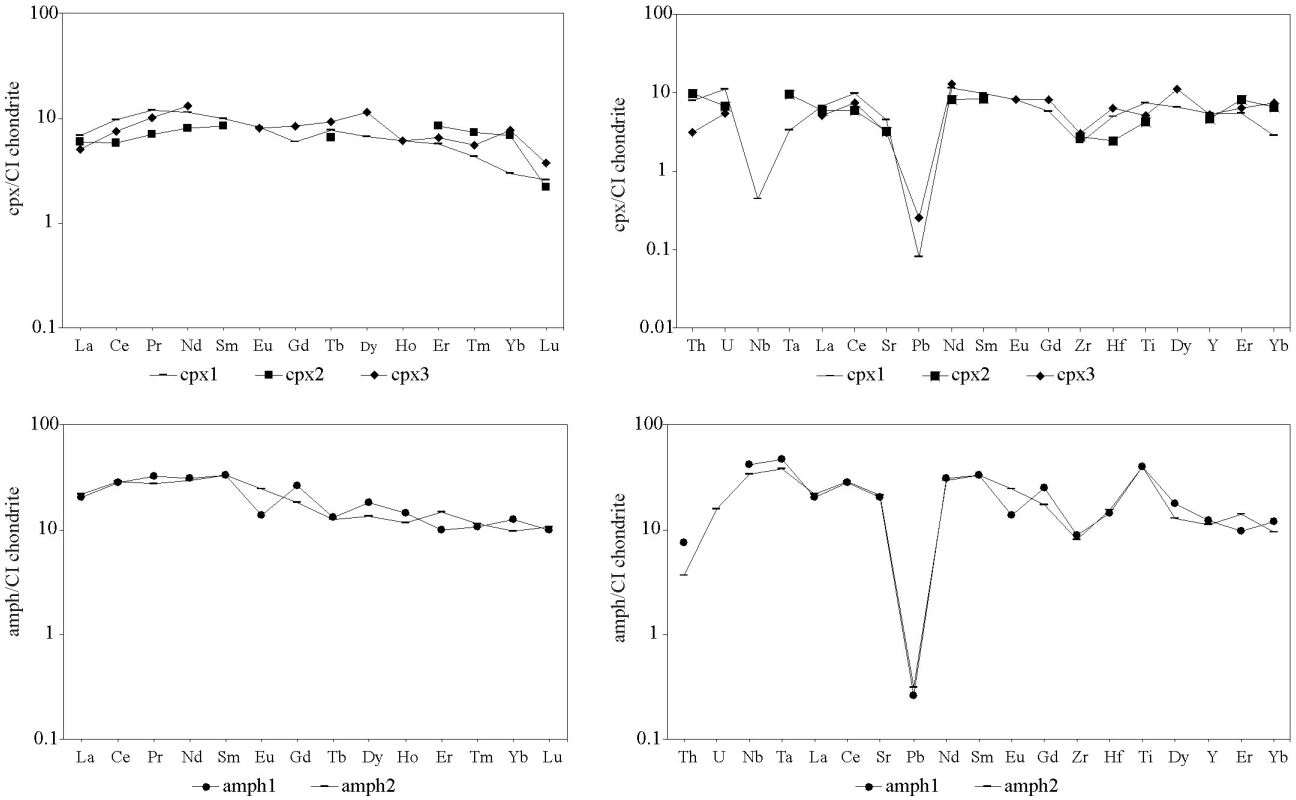

Figure 5. Chondrite-normalized REE and incompatible trace element patterns of the clinopyroxene and amphibole.

set of solid/liquid partition coefficients ($^{S/L}D$), the composition of the melt in equilibrium with the minerals can be calculated. Among the analyzed minerals clinopyroxene and amphibole are the most suitable to constrain the equilibrium melt compositions given their capability to incorporate a significant number of petrologically significant elements. The clinopyroxene/melt and amphibole/melt partition coefficients used in the calculations are from Adam and Green (2006) and Tiepolo et al. (2007), respectively. The N-MORB normalized incompatible trace element patterns of the melt compositions in equilibrium with clinopyroxene and amphibole are reported in Figure 6. The melts show almost similar patterns suggesting derivation from the same parental melts. The equilibrium melts are characterized by LREE enrichment over HREE (Ce_N/Yb_N=6.5 and 10.39 for average clinopyroxene and amphibole compositions respectively) and almost flat HREE pattern (Dy_N/Yb_N=0.80 and 1.05 for average clinopyroxene and amphibole respectively). Nb and Sr are depleted but Pb is enriched relative to the neighboring elements. As typical of subduction-related magmas, the two melts show a LILE enrichment over REE and Nb depletion relative to La.

Petrogenesis of the mafic rocks of the MPC

The whole rock trace element composition of the gabbro shows little variation (Figure 6a). Deevsalar et al. (2014, 2017) suggested that the gabbroic rocks crystallized from a melt evolved by fractional crystallization of olivine, pyroxene, amphibole, and plagioclase from a primitive magma assumed to be equivalent in composition to the MPC ultramafic rock (Figure 6a). Although the crystallization of olivine, clinopyroxene, amphibole, and plagioclase from this melt is capable to produce a new melt compositionally similar to the gabbro (Figure 7a), this process is unrealistic for the high proportion of solid phases that have to be crystallized (approximately 90%). Remarkably, even considering the increase of the $^{S/L}D$ for incompatible elements with melt differentiation (SiO_2), the required proportions of solid that have to be crystallized remains unrealistic. The high degree of fractional crystallization would produce an extremely SiO_2-rich residual melt characterized by low Mg#. However, the silica content and the Mg# of the gabbro are only slightly higher (~5%) and slightly lower (0.3), respectively, than those of the parental liquid. In addition, due to high compatibility of Ni and Co with olivine, amphibole and clinopyroxene, the residual melt is expected to be highly depleted in these elements and this is also not the

case. In the Harker-type variation diagrams (not shown) the ultramafic rocks (considered representative of the parental melt) deviates from the variation trend defined by the other samples likely for their cumulus origin. The approximation of their composition to that of a melt is thus an oversimplification. Moreover, the calculated composition of the melts in equilibrium with amphibole and clinopyroxene (which are almost concordant) do not resemble the whole rock composition of the gabbro for the lower abundances of MREE, HREE, Zr, Hf and Ti at comparable abundances of Ba, Rb, Nb, Ta and LREE (Figure 6a). This is a further evidence suggesting that also the bulk rock composition of the gabbro is not fully representative of the parental liquid.

In our attempt to understand the petrogenesis of the MPC gabbro, we looked for a rock type with a composition

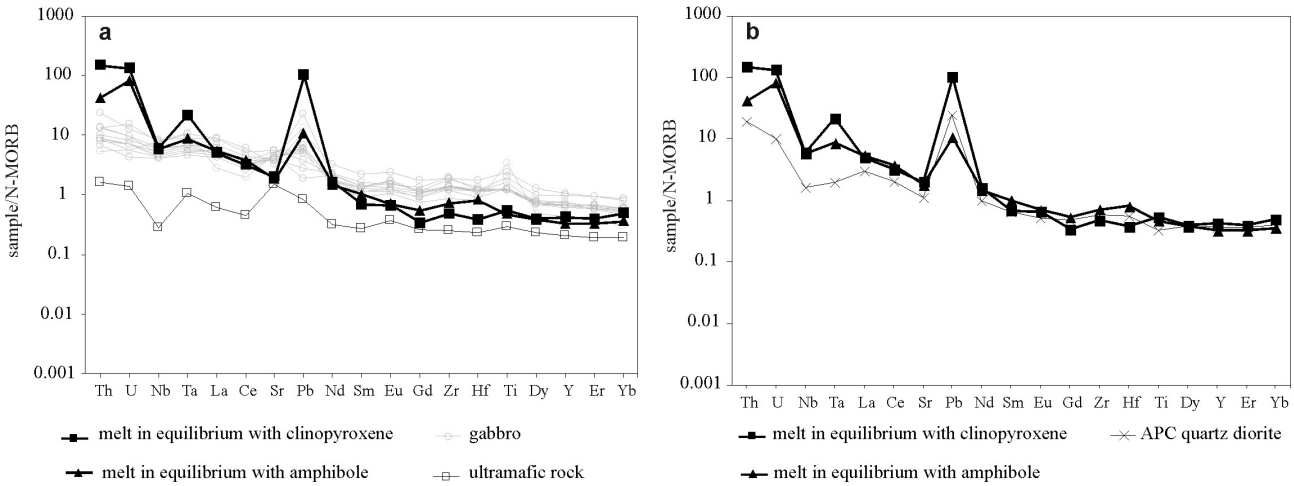

Figure 6. N-MORB normalized incompatible trace element patterns of the melts in equilibrium with average compositions of clinopyroxne and amphibole that are compared with a) the patterns for the gabbro and ultramafic rock (Deevsaral et al., 2014); b) the pattern for the APC quartz-diorite (Esna-Ashari et al., 2012).

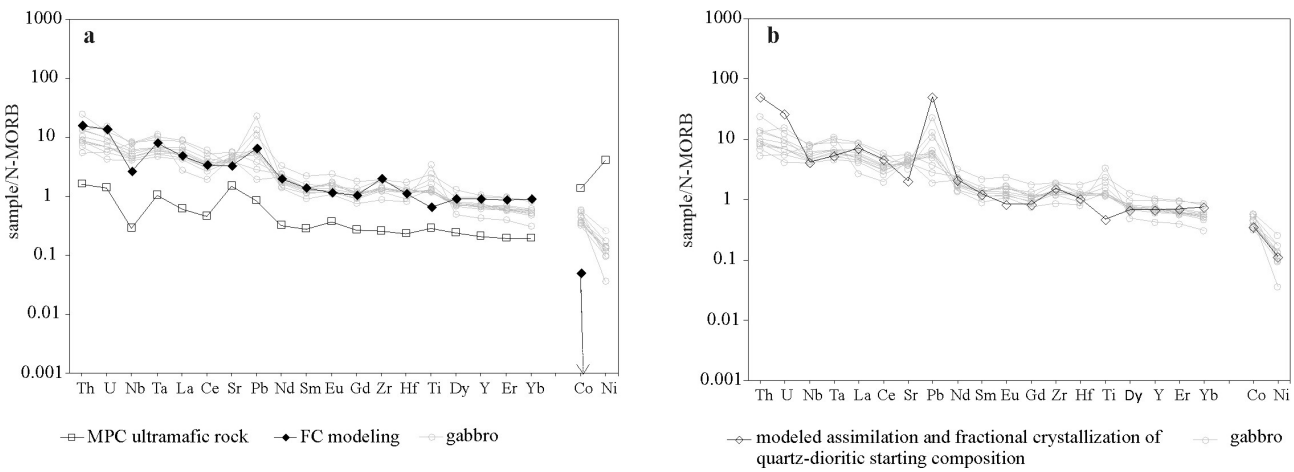

Figure 7. a) N-MORB normalized incompatible trace element pattern of the melt modeled with olivine, clinopyroxene, amphibole, and plagioclase fractional crystallization (FC) starting from the melt compositionally comparable with the ultramafic rock. The patterns of the gabbro (Deevsaral et al., 2014) are shown for comparison. Dashed line with the arrow shows that Ni content of the modeled melt is very lower than the range considered for the vertical axis of the diagram; b) N-MORB normalized incompatible trace element pattern of the melt modeled with assimilation and fractional crystallization (AFC). The starting composition proposed to be a melt comparable with APC quartz-diorite (Esna-Ashari et al., 2012). The patterns of the gabbro (Deevsaral et al., 2014) are shown for comparison. Mineral-melt partition coefficients that were used for the FC and AFC modeling are from Adam and Green (2006) and Tiepolo et al. (2007).

equivalent to that of the melt in equilibrium with clinopyroxene and amphibole and was identified in the intermediate quartz-dioritic rocks from the APC (Figure 6b). This similarity establishes a strong genetic link between the two plutonic complexes that is in agreement with the comparable ages and close location in the SSZ. Furthermore, clinopyroxene and amphibole from mafic to ultramafic rocks of the two complexes have comparable compositions (Figure 4). We can thus extrapolate to the MPC the genetic model proposed to account for the petrogenesis of the APC quartz-diorite.

Fractional crystallization coupled with melt-rock (ultramafic) reaction are the processes proposed to account for the chemical variations in the rocks of the northern half of the SSZ (Ahmadi-Khalaji et al., 2007; Esna-Ashari et al., 2011, 2012, 2014, 2016) and in particular in the case of APC and MPC rocks the two processes can be responsible for the apparently inconsistent higher SiO_2 and lower trace element contents of the quartz-diorite and the melts in equilibrium with clinopyroxene and amphibole) relative to the melt at the origin of gabbros (Figure 6). Fractional crystallization is retained responsible for the increase of SiO_2 in the residual melt whereas melt-ultramafic rocks interaction would buffer the increase of the incompatible trace element contents.

In the specific case of the MPC, we approximated the above processes to an assimilation and fractional crystallization (AFC) process in which we assumed the starting melt compositionally similar to the APC quartz-diorite and the assimilated material similar to the MPC ultramafic rock (troctolite-olivine gabbro; Deevsalar et al., 2014). Modeling shows that after about 60% fractionation of a mineral assemblage composed of olivine, clinopyroxene, amphibole, and plagioclase from the original magma and concomitant assimilation of the ultramafic rock, an evolved magma (richer in SiO_2 than the ultramafic rock) compositionally similar in the incompatible trace element content to the gabbro is produced (Figure 7b). It is assumed that relative ratio of assimilated material to crystallized material is equal to 0.5. This ratio agrees with the occurrence in the gabbro of xenolithic fragments mineralogically and texturally comparable with the assimilated ultramafic rocks (Figure 3d).

In order to better constrain the involvement of ultramafic rock in the differentiation process, we also considered compatible elements (e.g. Ni and Co) and Figure 8 shows that the modeled AFC process can account also for their observed variability.

In Figure 9 the evolutionary scenario for the formation of the MPC and APC mafic to intermediate rocks is summarized. Ultramafic rocks were emplaced at the first stage in Late Triassic to Early Jurassic times and subsequently in the Middle Jurassic they were intruded by an already evolved felsic melt. The interaction between this melt and the ultramafic rocks originated a new intermediate magma that evolved and gave origin to the MPC gabbroic rocks.

HMAs affinity of the MPC rocks

As outlined in the previous section many similarities between the MPC and the APC were found. Amphibole and clinopyroxene composition of the mafic to ultramafic rocks of the two complexes are comparable in composition (Figure 4). The MPC ultramafic rocks are compositionally very similar to those of the APC (Figure 10), that were proposed to be derived from a boninitic melt (Esna-Ashari et al., 2016). The same origin can be thus proposed for

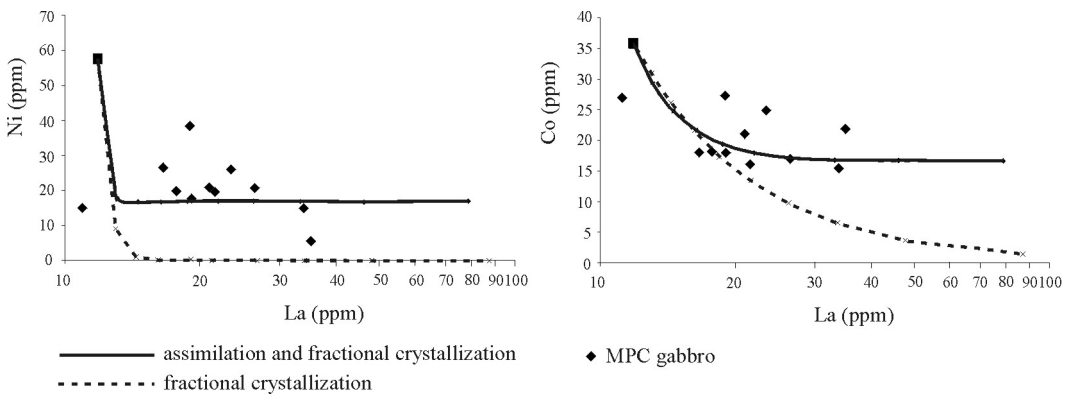

Figure 8. Ni and Co vs La variation diagrams for the MPC gabbro. Dashed and continuous lines represent the trends produced by FC and AFC processes respectively. APC quartz-diorite is considered as the starting composition. The length of the lines corresponds to 90% fractionation. Comparison of the two variation trends with the chemical variation of the MPC gabbro indicates that the AFC process can better explain the chemical variation of the samples.

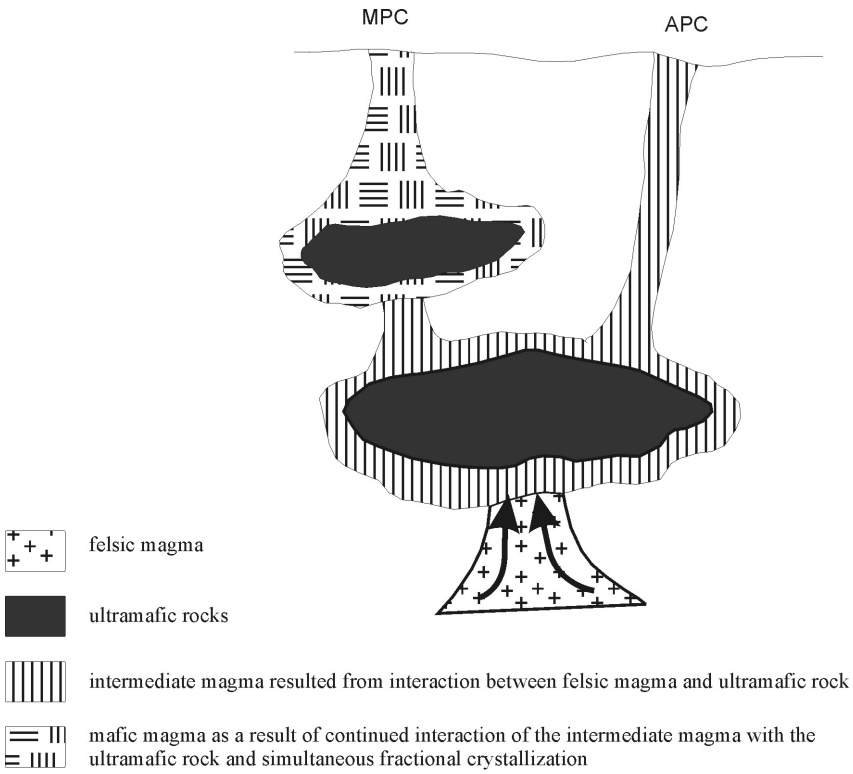

Figure 9. Cartoon showing the steps leading to the formation of the intermediate magma at the origin of the APC quartz-diorite and the mafic magma at the origin of the MPC gabbro. For details on the magma evolution processes, the reader is referred to the text.

both complexes. Melts in equilibrium with clinopyroxene and amphibole from MPC are also chemically comparable with the APC quartz-diorite that is classified as a generic HMA (Figure 6b; Esna-Ashari et al., 2016).

Here, in order to better characterize the geochemical affinity of high-Mg andesitic magma, we compared

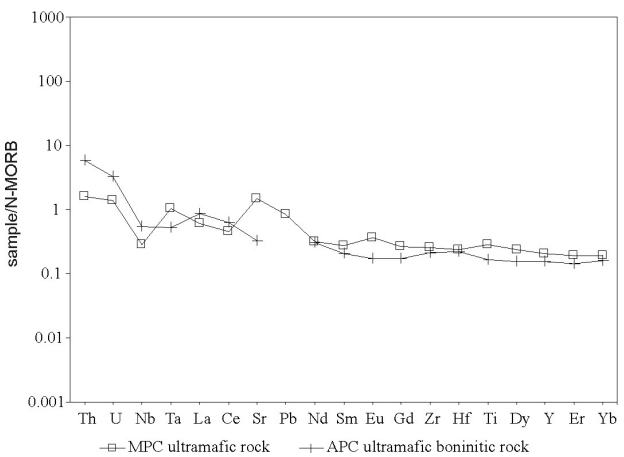

Figure 10. N-MORB normalized incompatible trace element patterns of the MPC ultramafic rock that is compared with the APC ultramafic rock with boninitic affinity (Esna-Ashari et al., 2016).

the compositions of the quartz-diorite and the melt in equilibrium with the analyzed minerals with the composition of the different HMAs types worldwide (Tatsumi and Ishizaka, 1982; Drummond et al., 1996; Shimoda et al., 1998; Smithies, 2000; Kelemen et al., 2003; Martin et al., 2005; De Oliveira et al., 2010). The comparison shows that HMAs from APC and MPC show different geochemical characteristics compared to boninites and adakites. Relative to the boninites they are enriched in incompatible elements and relative to the adakites they are slightly enriched in HREE and lack strong positive Sr anomaly. However, they closely resemble high-Mg andesitic magma with sanukitoid affinity (Figure 11; Tatsumi and Ishizaka, 1982; Shimoda et al., 1998; De Oliveira et al., 2010).

Sanukitoids are a group of HMA (mostly of Archean age) characterized by relatively high silica, MgO, Mg#, Cr, Na_2O, K_2O and LREE (e.g. Shirey and Hanson, 1984; Stern et al., 1989; Stern and Hanson, 1991). The genetic model proposed for the origin of the sanukitoids is the second-stage melting of a metasomatized peridotite for the addition of slab-melts (Rapp et al., 1999; Smithies and Champion, 1999). Here we do not pretend to propose an alternative genetic model for the Archean sanukitoids, however we have demonstrated that melts compositionally

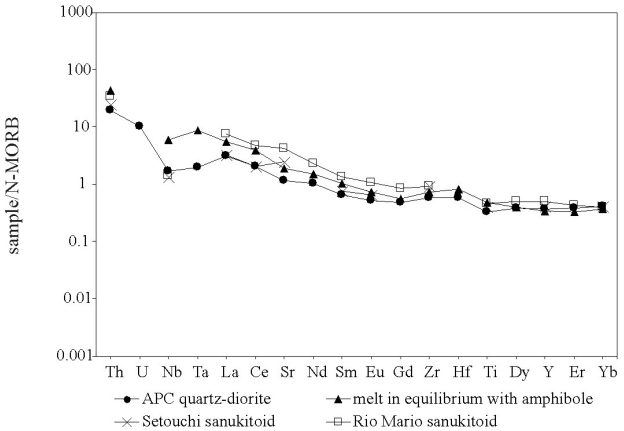

Figure 11. N-MORB normalized incompatible trace element patterns of the melt in equilibrium with amphibole and the APC quartz-diorite (Esna-Ashari et al., 2012) that are compared with Setouchi sanukitoid (Tatsumi and Ishizaka, 1982; Shimoda et al., 1998) and Rio Mario sanukitoid (De Oliveira et al., 2010).

similar to sanukitoids can be generated by the interaction between an already evolved felsic melt and pre-existing ultramafic rocks without invoking multiple partial melting events in the mantle source. In this frame, further studies should be aimed to better understand if Archean sanukitoids could represent products of melt-rock reaction.

CONCLUSIONS

The study of the gabbroic rocks from the Malayer pluton revealed that this complex is analogous to the neighbor Aligoodarz plutonic complex. In particular, two types of magma with high-Mg andesite affinity are distinguished in both complexes: a melt with boninitic composition at the origin of the ultramafic rocks and a melt with sanukitoid composition derived by the interaction between the former ultramafic boninitic rock and a later melt with more evolved composition.

The occurrence of ultramafic boninitic rocks also in the Malayer plutonic complex indicates that boninitic magmatism is more widespread in the northern half of the SSZ than previously thought. This suggests that the geodynamic setting necessary to cause the formation of boninite was prevailed in different parts of the SSZ during the onset of subduction in the Late Triassic-Early Jurassic.

This study also reveal the key role played by ultramafic rock at depth in the petrogenesis of intermediate melts in collisional settings.

ACKNOWLEDGEMENTS

The authors acknowledge the laser ablation lab of the CNR-IGG Pavia that funded the chemical analysis. Andrea Risplendente is acknowledged for the EMP analyses. Field sampling was financially supported by the research grant received from the Payame Noor University.

The quality of the paper was greatly improved by the editorial guidance and constructive reviews from an anonymous reviewer.

REFERENCES

Adam J. and Green T., 2006. Trace element partitioning between mica- and amphibole-bearing garnet lherzolite and hydrous basanitic melt: 1. Experimental results and the investigation of controls on partitioning behavior. Contributions to Mineralogy and Petrology 152, 1-17.

Agard A., Omrani J., Jolivet L., Whitechurch H., Vrielynck B., Spakman W., Monte P., Meyer B., Wortel R., 2011. Zagros orogeny: a subduction-dominated process. Geological Magazine 148, 692-725.

Ahadnejad V., Valizadeh M.V., Deevsalar R., Rezaei-Kahkhaei M., 2011. Age and geotectonic position of the Malayer granitoids: implication for plutonism in the Sanandaj-Sirjan Zone, W Iran. Neues Jahrbuch für Geologie und Paläontologie Abhandlungen 261, 61-75.

Ahmadi-Khalaji A., 2006. Petrology of the granitoid rocks of the Boroujerd area. Ph.D. Thesis, University of Tehran, Tehran, Iran.

Ahmadi-Khalaji A.A., Esmaeily D., Valizadeh M.V., Rahimpour-Bonab H., 2007. Petrology and geochemistry of the granitoid complex of Boroujerd, Sanandaj- Sirjan Zone, Western Iran. Journal of Asian Earth Sciences 29, 859-877.

Arvin M., Pan Y., Dargahi S., Malekizadeh A., Babaei A., 2007. Petrochemistry of the Siah-Kuh granitoid stock southwest of Kerman, Iran: implications for initiation of Neotethys subduction. Journal of Asian Earth Sciences 30, 474-489.

Berberian M. and King G.C.P., 1981. Towards a paleogeography and tectonic evolution of Iran. Canadian Journal of Earth Sciences 18, 210-265.

Crawford A.J., Falloon T.J., Green D.H., 1989. Classification, petrogenesis, and tectonic setting of boninites. In: Boninites and related rocks. (Ed.): A.J. Crawford, Unwin-Hyman, London, 1-49.

De Oliveira M.A., Dall'agnol R., Scaillet B., 2010. Petrological constraints on crystallization conditions of mesoarchean sanukitoid rocks, southeastern Amazonian craton, Brazil. Journal of Petrology 51, 2121-2148.

Deevsalar R., Ghorbani M.R., Ghaderi M., Ahmadian J., Murata M., Ozawa H., Shinjo R., 2014. Geochemistry and petrogenesis of arc-related to intraplate mafic magmatism from the Malayer-Boroujerd plutonic complex, northern Sanandaj-Sirjan magmatic zone, Iran. Neues Jahrbuch für Geologie und Paläontologie 274, 81-120.

Deevsalar R., Shinjo R., Ghaderi M., Murata M., Hoskin P.W.O., Oshiro S., Wang K.L., Lee H.Y., Neill I., 2017. Mesozoic-Cenozoic mafic magmatism in Sanandaj-Sirjan Zone, Zagros Orogen (Western Iran): Geochemical and isotopic inferences from Middle Jurassic and Late Eocene gabbros. Lithos 284-285, 588-607.

Deevsalar R., Shinjo R., Liégeois J.P., Valizadeh M.V., Ahmadian J., Yeganehfar H., Murata M., Neill I., 2018a. Subduction-related mafic to felsic magmatism in the Malayer-Boroujerd plutonic complex, western Iran. Swiss Journal of Geosciences 111, 269-293.

Deevsalar R., Shinjo R., Wang K.L., Yeganehfar H., Neil I., 2018b. Gabbroic-dioritic dykes from the Sanandaj-Sirjan Zone: windows on Jurassic and Eocene geodynamic processes in the Zagros Orogen, western Iran. Journal of the Geological Society, doi: https://doi.org/10.1144/jgs2017-156.

Defant M.J. and Drummond M.S., 1990. Derivation of some modern arc magmas by melting of young subducted lithosphere. Nature 347, 662- 665.

Drummond M.S., Defant M.J., Kepezhinskas P.K., 1996. Petrogenesis of slab-derived trondhjemite-tonalite-dacite/adakite magmas. Transactions of the Royal Society of Edinburgh: Earth Sciences 87, 205-215.

Esna-Ashari A., Tiepolo M., Hassanzadeh J., 2016. On the occurrence and implications of Jurassic primary continental boninite-like melts in the Zagros orogen. Lithos 258-259, 37-57.

Esna-Ashari A., Tiepolo M., Valizadeh M.V., Hassanzadeh J., Sepahi A.A., 2012. Geochemistry and zircon U-Pb geochronology of Aligoodarz granitoid complex, Sanandaj-Sirjan Zone, Iran. Journal of Asian Earth Sciences 43, 11-22.

Esna-Ashari A., Valizadeh M.V., Soltani A., 2014. Petrogenesis of microgranular enclaves in Aligoudarz granodiorite (in Persian). Iranian Journal of crystallography and mineralogy 22, 521-534.

Esna-Ashari A., Valizadeh M.V., Soltani A., Sepahi A.A., 2011. Petrology and geochemistry of Aligoodarz granitoid, Western Iran: implications for petrogenetic relation with Boroujerd and Dehno granitoids. Geopersia 1, 67-86.

Falloon T.J. and Danyushevsky L.V., 2000. Melting of refractory mantle at 1.5, 2, and 2.5 GPa under anhydrous and H_2O-undersaturated conditions: implications for the petrogenesis of high-Ca boninites and the influence of subduction components on mantle melting. Journal of Petrology 41, 257-283.

Hassanzadeh J. and Wernicke B.P., 2016. The Neotethyan Sanandaj-Sirjan zone of Iran as an archetype for passive margin-arc transitions. Tectonics, doi: 10.1002/2015TC003926.

Kay R.W., 1978. Aleutian magnesian andesites: melts from subducted Pacific ocean crust. Journal of Volcanology and Geothermal Research 4, 117- 132.

Kelemen P.B., 1995. Genesis of high Mg# andesites and the continental crust. Contributions to Mineralogy and Petrology 120, 1-19.

Kelemen P.B., Hangh, j.K., Greene A.R., 2003. One view of the geochemistry of subduction-related magmatic arcs, with an emphasis on primitive andesite and lower crust. In: The Crust. (Ed.): R.L. Rudnick, Elsevier, New York, 593-659.

Martin H., Smithies R.H., Rapp R., Moyen J.-F., Champion D., 2005. An overview of adakite, tonalite-trondhjemite-granodiorite (TTG), and sanukitoid: Relationships and some implications for crustal evolution. Lithos 79, 1-24.

Rapp R.P., Shimizu N., Norman M.D., Applegate G.S., 1999. Reaction between slab-derived melts and peridotite in the mantle wedge: experimental constraints at 3.8 GPa. Chemical Geology 160, 335-356.

Shahbazi H., Siebel W., Pourmoafee M., Ghorbani M., Sepahi A.A., Shang C.K., Vousoughi Abedini M., 2010. Geochemistry and U-Pb zircon geochronology of the Alvand plutonic complex in Sanandaj-Sirjan Zone (Iran): New evidence for Jurassic magmatism. Journal of Asian Earth Sciences 39, 668-683.

Shimoda G., Tatsumi Y., Nohda S., Ishizaka K., Jahn B.M., 1998. Setouchi high-Mg andesites revisited: geochemical evidence for melting of subducting sediments. Earth and Planetary Science Letters 160, 479- 492.

Shirey S.B. and Hanson G.N., 1984. Mantle-derived Archaean monozodiorites and trachyandesites. Nature 310, 222-224.

Smithies R.H., 2000. The Archaean tonalite-trondhjemite-granodiorite (TTG) series is not an analogue of Cenozoic adakite. Earth and Planetary Science Letters 182, 115-125.

Smithies R.H. and Champion D.C., 1999. Archaean high-Mg diorite (sanukitoid) suite, Pilbara Craton, Western Australia. In: The Origin of Granites and Related Rocks. (Ed.): B. Barbarin, Fourth Hutton Symposium Abstracts, September 1999. Clermont-Ferrand, France, p. 190.

Stern C.R. and Kilian R., 1996. Role of the subduction slab, mantle wedge and continental crust in the generation of adakites from the Andean Austral Volcanic Zone. Contributions to Mineralogy and Petrology 123, 263-281.

Stern R.J. and Hanson G.N., 1991. Archean High-Mg Granodiorite: A Derivative of Light Rare Earth Element-enriched Monzodiorite of Mantle Origin. Journal of Petrology 32, 201-238.

Stern R.J., 2002. Subduction zones. Reviews in Geophysics 40, 1012, doi:10.1029/2001RG000108, 2002.

Stern R.J., Hanson G.N., Shirey S.B., 1989. Petrogenesis of mantle-derived, LILE-enriched Archean monzodiorites and trachyandesites (sanukitoids) in southwestern Superior Province. Canadian Journal of Earth Sciences 26, 1688-1712.

Tatsumi Y. and Ishizaka K., 1982. Origin of high-magnesian andesites in the Setouchi volcanic belt, southwest Japan, I. Petrographical and chemical characteristics. Earth and Planetary Science Letters 60, 293-304.

Tiepolo M. and Tribuzio R., 2008. Petrology and U-Pb zircon geochronology of amphibole-rich cumulates with sanukitic affinity from Husky Ridge (Northern Victoria Land, Antarctica): insights into the role of amphibole in the petrogenesis of subduction-related magmas. Journal of Petrology 49, 937-970.

Tiepolo M., Oberti R., Zanetti A., Vannucci R., Foley S.F., 2007. Trace-element partitioning between amphibole and silicate

melt. Reviews in Mineralogy and Geochemistry 67, 417-452.
Tribuzio R., Tiepolo M., Fiameni S., 2008. A mafic-ultramafic cumulate sequence derived from boninite-type melts (Niagara Icefalls, northern Victoria Land, Antarctica). Contributions to Mineralogy and Petrology 155, 619-633.
Yogodzinski G.M., Kay R.W., Volynets O.N., Koloskov A.V., Kay S.M., 1995. Magnesian andesite in the western Aleutian Komandorsky region: implications for slab melting and processes in the mantle wedge. Geological Society of America Bulletin 107, 505-519.
Yogodzinski G.M., Volynets O.N., Koloskov A.V., Seliverstov N.I., Matvenkov V.V., 1994. Magnesian andesites and the subduction component in a strongly calc-alkaline series at Piip Volcano, far western Aleutians. Journal of Petrology 35, 163-204.